Annu. Rev. Mar. Sci. 2026. 18:X–X
https://doi.org/10.1146/annurev-marine-032123-025717

The Verification Challenge of Marine Carbon Dioxide Removal

Katja Fennel

Department of Oceanography, Dalhousie University, Halifax, Nova Scotia, Canada

Email: katja.fennel@dal.ca
ORCID: 0000-0003-3170-2331

Keywords

Carbon dioxide removal; ocean alkalinity enhancement; iron fertilization; artificial upwelling; macroalgal farming; air-sea flux

Abstract

It is increasingly obvious that, even when reaching net-zero emissions, removal of anthropogenic carbon dioxide (CO_2) from the atmosphere will be required. Some ocean-based removal technologies, while not proven for routine operation at scale, show promise. All of these rely on inducing a flux of CO_2 from the atmosphere into the ocean that is directly attributable to the removal intervention. Crucial for the economic viability of these technologies is the quantification of the cumulative net air-sea flux of CO_2 that an intervention can verifiably deliver. Because this flux is the difference between a realistic case with and a hypothetical case without intervention, it cannot be determined by observation alone. One must rely on a combination of informative observations and skillful models instead. Major uncertainties in quantification of net CO_2 uptake are the removal of seawater with a DIC deficit from direct contact with the atmosphere and the inevitable rebalancing of carbon among Earth's mobile carbon pools.

1. What is marine Carbon Dioxide Removal (mCDR)?

Global climate is warming at an accelerating pace because of anthropogenic activity, primarily the release of greenhouse gases due to combustion of fossil fuels and extensive changes in land use (IPCC 2023, Blunden & Boyer 2024). Although many consider halting global warming to be the most pressing environmental issue of our time, humanity's heavy reliance on fossil fuel-derived energy poses a significant hurdle to reducing greenhouse gas emissions. Increasingly, approaches for active removal of greenhouse gases from the atmosphere followed by their safe storage in other reservoirs is being considered as a necessary complement to emission reductions (IPCC 2018, 2023, Doney et al. 2025). Such approaches are referred to as Negative Emission Technologies (NETs). NETs that target carbon dioxide (CO_2), the largest contributor to global warming among the anthropogenic greenhouse gases, are referred to as Carbon Dioxide Removal (CDR) technologies.

CDR that relies on the ocean as a conduit for extracting CO_2 from the atmosphere is referred to as marine CDR (mCDR). mCDR technologies can be grouped broadly into abiotic and biotic approaches. Abiotic approaches do not rely on a manipulation of biological processes for carbon removal. They include the direct capture of CO_2 from seawater and the enhancement of ocean alkalinity either by adding alkaline minerals to or removing acidic constituents from seawater. Biotic approaches rely on a systematic alteration of biologically mediated fluxes. They encompass ocean fertilization with iron or macronutrients (including artificial upwelling), enhancement of biological carbon sinks in coastal systems (e.g., through restoration of seagrass meadows and mangroves), and farming and sinking of macroalgae in open ocean regions. Common to all mCDR approaches is their aim to induce a net flux of CO_2 from the atmosphere into the ocean by deliberate human intervention, i.e. the flux would not have occurred otherwise. This additional CO_2 flux through the air-sea interface is driven by a deliberate reduction of the partial pressure of CO_2 (pCO_2) in the surface ocean which changes the pCO_2 gradient between atmosphere and ocean thus inducing a net uptake. How the reduction in surface pCO_2 is accomplished varies by technology as does the form in which CO_2 is stored and thus the expected timescale of storage.

Several recent reports and reviews provide overviews of mCDR concepts including the status of current knowledge and related unresolved questions (NASEM 2022, Cooley et al 2022, Doney et al. 2025, Oschlies et al. 2025). This review focuses specifically on the challenge of quantifying the oceanic carbon uptake associated with mCDR activities—a critical aspect for verification by carbon markets. Palter et al. (2023) emphatically called for rigorous, transparent, and equitable protocols. The topic is actively discussed (Halloran et al. 2025, Bach et al. 2023, Fennel et al. 2023, Ho et al. 2023) but remains a work in progress.

2.1. Biotic mCDR approaches

Ocean fertilization aims to reduce surface ocean pCO_2 by stimulating photosynthesis. This is done by supplying either the micronutrient iron in regions where it is limiting or macronutrients outside of these regions. Iron fertilization would have to be applied in the high-nutrient, low-chlorophyll regions of the ocean (the Southern Ocean, the Subpolar North Pacific, and the Pacific Equatorial Upwelling region) where macronutrients are never completely exhausted because of a shortage of iron. Iron fertilization is thought to have contributed to the changes in atmospheric CO_2 that drove glaciations (Martin 1990) and is attractive among the nutrient fertilization concepts because the Fe:C stoichiometry is favorable. Although variable to within an order of magnitude (Sunda and Huntsman 1995), Fe:C stoichiometries in phytoplankton range from 2 to 13 µmol:mol or $2x10^{-6}$ to $1.3x10^{-5}$ mol:mol (Sunda 1997) which implies that adding 1 ton of iron could theoretically stimulate up to 100,000 tons of organic carbon production.

More than a dozen open-ocean iron fertilization experiments have been conducted since the idea was first proposed by John Martin (summarized in Boyd et al. 2007, Yoon et al. 2018). While these experiments have shown that the photosynthetic uptake of CO_2 can be enhanced by the addition of iron, thus driving an additional net flux of CO_2 into the ocean in the short term (Bakker et al. 2001), it is unclear how much of this additional carbon is sequestered in the deep ocean and how much is respired in the surface where it will outgas within months. Furthermore, it is likely that enhanced macronutrient drawdown in iron-fertilized patches leads to reduced productivity downstream, so-called nutrient robbing, which would at least partially offset CO_2 uptake—as has been shown in several modelling studies (Noh et al. 2024, Keller et al. 2014, Gnanadesikan et al. 2003, Sarmiento et al. 2004). Furthermore, modeling suggests that ceasing iron fertilization at any point in time would lead to substantial outgassing of the previously sequestered CO_2 (Jin et al. 2008, Keller et al. 2014), in other words, it may not deliver durable CDR. In addition to questions about the additionality of CDR delivered by iron fertilization and concerns over unintended consequences including nutrient robbing and exacerbation of ocean deoxygenation and ocean acidification (Strong et al. 2009), verification of carbon removal is a major challenge for this approach (NASEM 2022).

Fertilization with macronutrients via artificial upwelling seems conceptually fraught because the respiratory DIC content of seawater increases with depth in roughly the same proportion as inorganic macronutrient concentrations. This proportion happens to roughly match the stoichiometric requirements of photosynthetic microorganisms (Redfield et al. 1963, Anderson & Sarmiento 1994). In other words, pumping seawater from the ocean interior to the surface in the hope that macronutrients stimulate photosynthesis to take up atmospheric CO_2 neglects the fact that the same water contains elevated DIC. To first order, one would expect a zero-sum effect with regard to air-sea exchange of CO_2 where upwelled DIC is sufficient to meet the photosynthetic demands of phytoplankton. More elaborate causalities have been proposed, e.g., stimulation of diazotrophic phytoplankton (Karl & Letelier 2008) which do not strictly depend on fixed nitrogen (the proximate limiting macronutrient in most of the ocean) and thus could grow until residual phosphate (the ultimate limiting macronutrient in the ocean) is exhausted. This proposed approach aims to exploit a relatively small deviation from average stoichiometries between carbon, nitrogen and phosphorus and relies on the success of specialized microbes that is hard to predict and even harder to control making it unlikely to reliably deliver CDR and operate on the scales required (Fennel 2008). Furthermore, artificial upwelling, if implemented on a large scale, would work to erode ocean stratification with implications for the ocean's productivity and heat balance that would run counter to the goal of mitigating global warming (Fennel 2008, Keller et al. 2014, Oschlies et al. 2010, Yool et al. 2009).

Farming of macroalgae, multicellular photosynthetic organisms commonly referred to as seaweed, followed by sequestration of the resulting biomass in the deep ocean has been proposed to induce a net flux of atmospheric CO_2 into the ocean. This approach requires a deliberate strategy to induce sinking of macroalgal biomass (e.g. by compacting). A notable difference to the fertilization approaches described above, which would stimulate phytoplankton, is that the C:N ratio of macroalgae is higher (Sheppard et al. 2023), implying that more organic carbon per unit of available macronutrients could be produced and potentially removed. However, even under optimistic assumptions and assuming global implementation, the estimated CO_2 removal potential by macroalgal farming is small (0.1 gigatons per year according to Koweek 2022) and concerns over downstream nutrient robbing, unintended impacts on deep-sea sediments, and exacerbation of ocean deoxygenation and ocean acidification still apply (Bach et al. 2021). This approach, if implemented at scale, would entail a major modification of marine ecosystems (Boyd et al. 2022) with possibly major unintended consequences. Verification of carbon removal would also be a formidable challenge for this approach.

In principle, a biotically induced net flux of CO_2 from the atmosphere into the ocean can be achieved without stimulating photosynthesis by avoiding the release of respiratory CO_2. For example, a conversion of labile forms of dissolved organic carbon (DOC) into more refractory forms could reduce the release of respiratory CO_2 from microbially or photo-oxidatively degraded DOC to the atmosphere and thus increase the ocean's pool of DOC (Jiao et al., 2014). Because it is not obvious how this could be accomplished deliberately and on a large scale, verification of this approach is not discussed further.

The abovementioned biotic approaches can be thought of as an acceleration of the biological carbon pump (BCP, Oschlies et al. 2025). The BCP refers to a collection of physical transport and biological transformation processes that result in the long-term storage of biologically derived carbon in the ocean. Sometimes, the BCP is conflated with the transfer of photosynthetically produced organic carbon from the sunlit surface ocean to its interior. However, it is important to note that a stimulation of photosynthetic uptake does not in itself equate to an acceleration of the BCP. The same is true for a reduction in respiratory loss of organic matter to CO_2. The BCP results in changes in ocean carbon storage only if the net result of an altered downward flux of POC and the upward flux of remineralized carbon is changed (Frenger et al. 2024). If, for example, an increase in the downward flux of organic carbon is compensated by an increase in the upward flux of remineralized DIC, no increase in the pool of sequestered carbon would result and the magnitude of the BCP would remain unchanged. Analogously, a reduction in the respiratory return of CO_2 could be compensated for by a decrease in photosynthetic production, which is plausible since photosynthesis is partly fueled by nutrients stemming from remineralized labile DOC.

Acceleration of the BCP via mCDR thus hinges on a net increase in the downward flux of carbon or a net decrease in the upward return flux of carbon or both.

Restoration or creation of vegetated coastal habitats, i.e. mangroves, salt marshes, and seagrass meadows, is also being discussed as a biotic mCDR approach because these habitats hold significant amounts of organic carbon in their soils and seabeds. Vegetated coastal habitats make up about 0.5% of the ocean's surface (Macreadie et al. 2021) and have been severely decimated due to coastal development. While coastal restoration would deliver many benefits (including protection from erosion and ecosystem benefits such as nursery grounds), its potential as a carbon removal approach is estimated to be small (Gattuso et al. 2018). Verification of additional carbon uptake by this approach would be difficult (Williamson & Gattuso 2022) and require qualitatively different approaches than verification of other mCDR approaches. Therefore, it will not be discussed further in this review.

2.2. Abiotic mCDR approaches

Abiotic mCDR approaches aim to reduce the surface ocean's pCO_2 directly, either by enhancing its alkalinity, thus increasing the amount of CO_2 that a given volume of seawater can hold at equilibrium with the atmospheric pCO_2, or by extracting CO_2, which has to be stored elsewhere.

Ocean alkalinity enhancement (OAE) promises high durability and has a large potential for scale-up (Renforth & Henderson 2017). Several approaches have been proposed and are under active investigation (Eisaman et al. 2023, Oschlies et al. 2025). One involves addition of lime (as quick lime, hydrated lime [Kheshgi 1995], or ikaite [Renforth et al. 2022]), others the addition of pulverized silicate or carbonate rocks, or material derived from rocks such as concrete or steel slag (Rau & Caldeira 1999, Caldeira & Rau 2000, Harvey 2008, Renforth & Henderson 2017, Renforth 2019). In contrast, the electrochemical approaches do not add minerals but instead extract acids from seawater, thus enhancing its alkalinity (House et al. 2007, Rau 2008, Rau et al. 2013).

Ongoing research & development on OAE is focused on practical aspects of implementation and on potential unintended effects on ecosystems. Practical aspects include sourcing and processing of suitable feedstock (including the associated energy demands; Foteinis et al. 2022), evaluating the tradeoffs of different modes of dispersal and whether minerals dissolve fast enough or sink out of the surface ocean (Yang & Timmermans 2024, Wang et al. 2025), the risk of spontaneous secondary precipitation (Moras et al. 2022, Hartmann et al. 2023) which would remove alkalinity and is more acute for approaches which can induce large pH spikes (i.e. liming and electrochemical methods), finding a safe use or disposal method of the large quantities of acids that would be produced if electrochemical OAE were implemented at gigaton scale (Eisaman et al. 2023), and quantification of the net CO_2 uptake. Concerns about unintended ecosystem impacts are relevant for mineral feedstocks, because they include varying amounts of silicate and trace metals that would be introduced to seawater. These may affect marine organisms from primary producers to high trophic-level species either enhancing their productivity or posing risks (Guo et al. 2024, Ferderer et al. 2024, Garai et al. 2021, Montserrat et al. 2017).

In direct removal, CO_2 is extracted from seawater via electrochemical methods (Saha et al. 2024, Seo et al. 2024) for long-term storage in a geological reservoir. This approach is similar to direct air capture of CO_2 in terms of long-term storage. However, there is an important difference that makes direct CO_2 removal from seawater an mCDR technique, namely the reliance on a net air-sea flux resulting from the deliberate lowering of seawater pCO_2. While the removal of CO_2 from seawater occurs in a closed system and can be accurately quantified, no net removal of CO_2 from the atmosphere occurs until after the treated seawater is released back into the ocean and its relative DIC deficit resulting from the CO_2 capture is replenished by CO_2 uptake from the atmosphere. Thus, the quantification of this uptake is necessary, as for all the other mCDR techniques discussed above, and poses similar challenges.

3. The MRV challenge

Two necessary characteristics of any viable mCDR technology are that an additional net flux of CO_2 from the atmosphere into the ocean must be induced that would not have occurred without the CDR intervention—this is referred to as additionality—and that the added CO_2 is stored in the ocean or its sediments for a sufficiently long time. The additional CO_2 flux through the air-sea interface is driven by a deliberate reduction of the surface ocean's pCO_2 which modifies the pCO_2 gradient between atmosphere and ocean thus effecting a change in air-sea flux. The reduction in surface ocean pCO_2 can be thought of as the creation of a DIC deficit, noting that local temperature, salinity, background DIC, and background alkalinity affect the ratio of pCO_2 to DIC. How the reduction in surface pCO_2 is accomplished varies by technology as does the form in which CO_2 is stored and thus the expected durability of storage.

Quantification of the net flux of CO_2 is central to its verification for carbon markets and the main subject of this review. How this should be accomplished is actively discussed in the recent literature as well as among practitioners and verifiers and remains an open question (Halloran et al. 2025). While it is relatively easy to define general criteria that have to be met for satisfactory verification (i.e. durability, additionality, minimal negative impacts on ecosystems), it is much more difficult to articulate concrete procedures and metrics for evaluating these criteria and to define quantitative thresholds that have to be met for each criterion to be satisfied. In other words, it is difficult to set reasonable standards. Verification also requires a full accounting of CO_2 and other greenhouse gases emitted in the course of the CDR activity, e.g. in the production, processing, and transport of feedstock or the installation and operation of dedicated infrastructure, in a life cycle analysis (LCA; Foteinis et al. 2022, Butnar et al. 2024). However, the aim here is to discuss the sequence of processes that starts with the manipulation of seawater to induce net uptake of CO_2 and onward.

Aspects that have to be considered are: 1) the relative deficit in seawater DIC that is induced by the CDR activity, 2) the temporal evolution of the integrated net flux of CO_2 from the atmosphere into the ocean as a result of the induced DIC deficit, 3) any return fluxes of CO_2 and other greenhouse gases to the atmosphere, and 4) possible environmental harms or co-benefits. The first three will be discussed in detail below. Discussion of the fourth, beyond that written in section 2.1., is outside of the intended scope of this review but are examined elsewhere (Oschlies et al. 2025, Roberts et al. 2025).

The DIC deficit that is introduced by a specific CDR activity represents the "maximum possible CDR" or "potential CDR" that can be achieved by this activity. The efficiency of a specific intervention is the ratio between the accomplished net CO_2 uptake that has occurred within a reasonable timeframe (subsequently also referred to as the realized CDR or CDR(*t*)) and the potential CDR. Up to 10 or 15 years may be considered reasonable, while 100 to 1,000 years would not. This definition of efficiency is equivalent to the definition of cumulative additionality by Yamamoto et al. (2024). It does not consider air-sea fluxes of greenhouse gases other than CO_2 that may be induced by the CDR intervention. Although CDR(*t*) may approach the maximum possible amount (i.e. the DIC deficit induced by the intervention) within a few years, leakage of CO_2 from different reservoirs in the Earth system into the atmosphere will occur in the long term due to a repartitioning of carbon between Earth's mobile carbon reservoirs (Oschlies 2009, Keller et al. 2014, Yamamoto et al. 2024, Tyka 2025). The potential emissions of other greenhouse gases and long-term leakage of CO_2 should be considered when verifying CDR interventions.

It is important to note that quantifying these aspects requires consideration of two scenarios: the realistic case, where the ocean is subjected to a CDR intervention, and the counterfactual case, where this intervention did not happen. Thus, the relative DIC deficit induced by the intervention is the difference between a real, observable state and a hypothetical state that cannot be observed. The same holds true for the net air-sea flux of CO_2 and any leakage induced. This fact presents a challenge to verifying CDR in that multiple aspects are not observable by definition yet have to be quantified.

3.1. Relative DIC deficit in seawater induced by CDR

Since the mechanisms by which a relative DIC deficit is induced in surface waters differ by approach, so does the effort involved in quantifying this deficit.

For OAE, the induced DIC deficit is directly related to the amount of added alkalinity. This is relatively straightforward to quantify for electrochemical methods because removal of acids occurs in a closed system and can be measured directly. For mineral-based OAE, the amount of alkalinity added is more difficult to assess. A minor issue is that feedstocks contain impurities. These can be accounted for through careful analysis of feedstock composition. A bigger complication is that complete dissolution of feedstock cannot be assumed a priori (Wang et al. 2025). In open-ocean applications, loss of feedstock due to sinking would reduce the ratio of potential to realized CDR, i.e. the efficiency of the process (Yang and Timmermans 2024). In coastal applications, feedstock may accumulate on the seabed and be incorporated into sediments without enriching the overlying water column in alkalinity (Bach 2024, Wang et al. 2025). Assuming the amount of added alkalinity, which we refer to as $[\mathrm{Alk}]_{\mathrm{added}}$, has been quantified, the relative DIC deficit is equal to $\eta[\mathrm{Alk}]_{\mathrm{added}}$ where η is the isocapnic quotient (Humphreys et al. 2018) or CO_2 uptake factor (Schulz et al. 2023). Some authors have attached a slightly different meaning to η and referred to it as the time-dependent efficiency of alkalinity enhancement (He & Tyka 2023, Tyka 2025, Yankovsky et al. 2024, Zhou et al. 2025). Here, a more generally applicable definition of efficiency is used (see box 1). One complication in converting added alkalinity to a DIC deficit is that η is not a constant but depends on local seawater characteristics, primarily temperature, and varies between 0.77 and 0.96 with higher values found closer to the poles (Schulz et al. 2023).

For biotic CDR, a relative CO_2 deficit can arise because of an increase in the downward flux of organic carbon. Quantification of such CO_2 deficit would require a determination of how much additional organic carbon sinks out of the surface ocean above and beyond the downward flux that would occur without the CDR intervention, i.e. the baseline. Current estimates of the baseline vertical flux of organic matter are very imprecise. Direct observations via particle traps and thorium isotopes are sparse and heavily biased toward the northern hemisphere and upper 500 m of the ocean (Mouw et al. 2016, Doney et al. 2024). Climate model estimates of the globally averaged vertical flux of organic matter range from 5 to 12 Gt of CO_2 per year at present (Henson et al. 2022) and their simulated vertical transport of organic matter differs quantitatively and shows qualitatively different latitudinal patterns (Wang & Fennel 2024).

The depth to which the additional organic carbon sinks before it is respired, and ocean circulation, determine the timescale of CO_2 storage. Carbon stored below 1,000 m is considered sequestered for over 100 years (Siegel et al. 2021), although shallower respiration may also meaningfully contribute to ocean carbon sequestration (Ricour et al. 2023). Quantification of timescales of storage largely relies on model simulations.

Given current capabilities for observing the naturally occurring downward flux of organic carbon in the ocean and the current state of biogeochemical ocean models, it seems unlikely that the differential flux can be quantified with confidence. Assuming, for the sake of argument, that it could be, then the relative CO_2 deficit induced by iron fertilization or macroalgal farming would be equal to the additional organic carbon exported to a sufficient depth—what depth would be considered sufficient remains to be determined. When organic matter export is stimulated by macronutrient fertilization through artificial upwelling, one needs to account for the upwelled DIC, which reduces any DIC deficit resulting from enhanced organic matter export. In the case of iron fertilization, it may be tempting to convert the added micronutrient into additional organic matter export assuming stoichiometric ratios; however, an increase in organic matter production is not necessarily equal to an increase in vertical carbon flux and the stoichiometries for converting iron to carbon are highly variable.

3.2. Net air-sea flux of CO_2

The relative DIC deficit induced by an intervention sets an upper limit for CDR that can occur. How much of this potential CDR is realized, i.e. the efficiency of the intervention, depends on the net air-sea flux from the atmosphere into the ocean that is effected by the deficit.

Several authors have made the point that "quantification via measurement" is not an option for the net CO_2 flux, because of the fast dilution/dispersion of any induced DIC deficit and because of unfavorable signal-to-noise ratios in DIC and pCO_2, and thus must rely on models (Bach et al. 2023, Ho et al. 2023, Palter et al. 2023, Tyka 2025). A more fundamental reason, that may seem obvious but has not been clearly articulated before, is that, by definition, the counterfactual cannot be directly measured. Quantification of the net flux must therefore rely on skillful biogeochemical models (see Fennel et al. [2022] for a primer). Despite the necessary reliance on models for quantification of the net CO_2 flux, the importance of measurements for rigorous validation, tuning, and uncertainty assessments of models as well as for model-data fusion via data assimilation has been stressed (Watson et al. 2008, Fennel et al. 2023). A parallel can be drawn to operational ocean modelling, where observing system simulation experiments (OSSEs) are common. Like in MRV, OSSEs rely on the quantification of differences between two simulations and have been shown to yield misleading results when the models are biased or inaccurate (Yu et al. 2019). Clear minimum criteria, based on years of intensive research and learning, have been articulated for OSSEs (Halliwell et al. 2014) but are not yet available for CDR quantification.

Since the air-sea equilibration of CO_2 is relatively slow—Jones et al. (2014) estimate the area-weighted global annual mean equilibration timescale as 4.4 ± 3.4 months—the efficiency depends critically on how long seawater with a DIC deficit is in contact with the atmosphere. Several recent global and regional modelling studies have begun to address quantification of this aspect for OAE. He and Tyka (2023), Yamamoto et al. (2024), and Zhou et al. (2025) simulated OAE interventions in their global models and evaluated CDR efficiency in different locations. Their results show regional and seasonal dependencies but generally suggest close to the maximum possible efficiency is reached within 5 to 15 years. With horizontal resolutions ranging from 0.3 to 2 degrees latitude these models are, at best, eddy permitting. Even in the mesoscale, which is beginning to be resolved by some of these models, transport is largely horizontal, with the largest eddies dominating the stirring and stretching of tracer filaments (Doney et al. 2025). However, when submesoscale processes are resolved, large vertical velocities can occur (Mahadevan 2016, McWilliams 2016) that may effectively remove seawater with a DIC deficit from the mixed layer (Doney et al. 2025). Such vertical transport via mixing and subduction reduces CDR efficiency but is yet to be reliably quantified. Re-entrainment of seawater with a DIC deficit is also possible and should be considered.

Bach et al. (2023) have called for gridded products of CDR efficiency for verification purposes and Zhou et al. (2025) have provided global maps of time-evolving CDR relative to localized alkalinity perturbations, i.e. a global set of time-dependent CO_2 uptake curves, which they refer to as impulse-response functions (IRFs). Yankovsky at al. (2024) further expanded on this concept, proposing IRFs as characteristic uptake curves that may serve, through linear combination, as a general solution to quantifying the efficiency of net air-sea flux. This would require the net air-sea flux to be linear relative to perturbations and time-invariant—assumptions that are not exactly met (Yankovsky at al. 2024) and not supported by the simple assessment presented in section 4. Leaving the validity of IRFs for generalized CDR verification aside, a rigorous assessment of their accuracy, even when explicitly calculated for a specific case, remains outstanding. Model intercomparisons and model ensembles are one approach for evaluating uncertainty (Keller et al. 2018, Fennel et al. 2023). It is often assumed that an ensemble mean is more accurate than most individual ensemble members because by combining models with complementary strengths, errors may average out. The underlying assumption is that ensemble members deviate randomly from reality without systematic biases. Often this is not the case, e.g. for CMIP models (Laurent et al. 2021). Ensembles only yield reliable uncertainty estimates if the sources of error leading to ensemble spread reflect the true and unbiased uncertainty in the real system that is simulated by the model ensemble. In practice, this is difficult to assess and ensure although several approaches have been developed in the context of operational ocean modelling, e.g. rank histograms. Like ensembles, model intercomparisons without rigorous validation against high-quality, appropriately resolved observations are not sufficient for quantifying model uncertainty.

3.3. Long-term return fluxes of greenhouse gases

Further to assessing the CO_2 deficit, which is created immediately following a CDR intervention, and the resulting net uptake of CO_2 from the atmosphere that occurs within 5 to 15 years of the intervention, there will be a long-term return flux of CO_2 to the atmosphere due to an inevitable rebalancing among Earth's mobile carbon pools and possibly the release of other greenhouse gases. These long-term return fluxes should be quantified and considered when verifying CDR interventions as they reduce the climatic benefit gained by the initially induced ocean uptake of CO_2.

Several modelling studies have assessed mCDR approaches assuming a fixed atmospheric pCO_2, essentially equivalent to an infinite atmosphere (He & Tyka 2023, Wang et al. 2023, Zhou et al. 2025). These simulations overestimate the CDR-induced air-sea flux because they do not account for the reduction in atmospheric pCO_2 that occurs due to CDR and any subsequent rebalancing (Oschlies 2009, Oschlies et al. 2010, Keller et al. 2014, Yamamoto et al. 2024, Jeltsch-Thömmes et al. 2024, Tyka 2025). Any change in distribution among Earth's mobile carbon pools leads to a long-term readjustment among them. Keller et al. (2014) assessed a range of CDR approaches and solar radiation management with an Earth system model that includes the land biosphere and showed that such readjustment occurs, to varying degrees, for all approaches. Yamamoto et al. (2024), in a fully coupled ocean-atmosphere model, estimated that CDR efficiency, after an initially rapid increase over a few years to decades, decreases to 50% at best after 100 years. Jeltsch-Thömmes et al. (2024), employing probabilistic observation- constrained ensembles of two Earth system models, found efficiencies of OAE to be less than 50% because of weakened carbon sinks on land and in the ocean due to the CDR intervention (in some cases sinks turned to sources). Importantly, the underlying redistribution among carbon pools is not characteristic of just mCDR. It also occurs for direct air capture (Yamamoto et al. 2024) and any decarbonization efforts that reduce CO_2 emissions because only about half of present-day emissions stay in the atmosphere with the remainder removed by land and ocean sinks.

Several authors have measured mCDR efficiency relative to that of direct air capture of CO_2 (Yamamoto et al. 2024, Tyka 2025) because the latter can be considered as the close to ideal case with respect to efficiency, given that CO_2 is directly removed from the atmosphere. This is a useful comparative metric of efficacy because it removes the complication of carbon redistribution throughout the Earth system but should not distract from the imperative of considering the redistribution in verification. Consideration of long-term CDR efficiency is further complicated by its dependence on emission pathways (Schwinger et al. 2024, Jürchott et al. 2023).

4. Simple case studies

The common aspect to all mCDR approaches, and of first order importance for assessing their efficiency, is the integrated net air-sea flux of CO_2. Several questions related to the quantification of this flux are investigated quantitatively here with the help of an idealized model. The simulations presented here assume the relative DIC deficit is created through OAE, but the model can be applied easily to other mCDR approaches. Furthermore, the atmospheric pCO_2 is fixed here, assuming an infinite atmosphere, but the model can easily be modified to assess the implications of a finite atmosphere.

When taking a Lagrangian view, idealized equations for the time-rate-of-change of DIC and alkalinity (Alk) in a surface parcel of seawater can be written as

$$\partial \mathrm{DIC}(\mathbf{x},t)/\partial t = -\, k \cdot \nabla^2 \mathrm{DIC}(\mathbf{x},t) - \tau_v\,(\mathrm{DIC}(\mathbf{x},t) - \mathrm{DIC}^{deep}) + F(\mathrm{DIC},\mathrm{Alk}), \text{ and} \quad (1)$$

$$\partial \mathrm{Alk}(\mathbf{x},t)/\partial t = -\, k \cdot \nabla^2 \mathrm{Alk}(\mathbf{x},t) - \tau_v\,(\mathrm{Alk}(\mathbf{x},t) - \mathrm{Alk}^{deep}), \quad (2)$$

where $\mathbf{x}$ is a point in space, t is time, k is the dispersion coefficient, τ_v is the vertical mixing timescale, DIC^{deep} and Alk^{deep} are background concentrations in the deep ocean, and F is the air-sea flux of CO_2, which depends on the windspeed, temperature, salinity, Alk, DIC, and the air pCO_2 and is only applicable when the water parcel resides at the sea surface. Assumptions are made here that advection and dispersion are distinct processes, that advection leads to a horizontal translation of the water parcel only but does not affect its shape, that horizontal dispersion is isotropic, and vertical advection is ignored. With these assumptions in a Lagrangian reference system that moves with the water parcel, there is no need to account for horizontal advection explicitly.

To estimate the amount of CO_2 removed from the atmosphere due to a CDR intervention, one needs to calculate the difference between the realistic case with intervention and the corresponding counterfactual without it. Henceforth, the tracer variables DIC and Alk correspond to the realistic case and DIC^{cf} and Alk^{cf} to the counterfactual. One then has to consider two pairs of tracer equations, pair 1 and 2 from above, and

$$\partial DIC^{cf}(\mathbf{x},t)/\partial t = - k \cdot \nabla^2 DIC^{cf}(\mathbf{x},t) - \tau_v (DIC^{cf}(\mathbf{x},t) - DIC^{deep}) + F(Alk^{cf},DIC^{cf}), \text{ and} \quad (3)$$

$$\partial Alk^{cf}(\mathbf{x},t)/\partial t = - k \cdot \nabla^2 Alk^{cf}(\mathbf{x},t) - \tau_v (Alk^{cf}(\mathbf{x},t) - Alk^{deep}). \quad (4)$$

A numerical representation of this model was coded in Matlab using the carbonate chemistry routines from Zeebe and Wolf-Gladrow (2001) and is available on github (Fennel 2025).

The CO_2 uptake at time t due to a CDR intervention, referred to here as the realized CDR, is

$$CDR(t) := \Sigma DIC(t) - \Sigma DIC^{cf}(t),$$

where Σ refers to the spatial integral over the whole ocean. Because the rebalancing of CO_2 between ocean and atmosphere is ignored here (i.e. atmospheric pCO_2 is constant) CDR(t) grows monotonically in time. Thus, a maximum realized CDR can be defined as

$$CDR^{max} := \lim_{t \to \infty} CDR(t).$$

In realistic cases, CDR(t) does not grow monotonically, and the maximum realized CDR is achieved at a specific point in time that is difficult to determine. For a monotonically growing CDR(t) one can define a timescale for measuring progress toward achieving CDR^{max} as $t_{x\%}$ which is the time until x% of CDR^{max} is realized, i.e. $CDR(t_{x\%}) = x/100 \ CDR^{max}$.

The efficiency of a CDR intervention, $\varepsilon(t)$, is the ratio of CDR(t) to $[DIC]_{deficit}$, the DIC deficit induced by the intervention. In biotic model cases, $[DIC]_{deficit}$ could be a prescribed removal of DIC, i.e. an input variable. For OAE, the DIC deficit is related to the prescribed alkalinity addition via the isocapnic quotient, η, as $[DIC]_{deficit} = \eta[Alk]_{added}$. Ideally the efficiency will approach 100%, in other words CDR(t) will approach $[DIC]_{deficit}$, in a short time. This is true for some of the idealized model cases below, but never the case for realistic applications where the DIC deficit represents an upper limit for CDR that cannot be reached because of inefficiencies in the net air-sea flux and an inevitable rebalancing of carbon among its mobile pools.

4.1. Case 1: The surface ocean as a homogenous box

The simplest case is a homogenous, fully mixed surface ocean that is in exchange with a homogenous, fully mixed atmosphere and subjected to an OAE intervention at time $t = 0$. It follows from the assumption of homogeneity that dispersion does not have to be considered and that there is no need for a spatial dimension, just time. Equation 1 simplifies to $\partial\mathrm{DIC}(t)/\partial t = \mathrm{F}(\mathrm{DIC})$ and equation 2 becomes trivial for $t > 0$, i.e. $\partial\mathrm{Alk}(t)/\partial t = 0$. In this case, $\mathrm{DIC}^{\mathrm{equib}}$ and $\mathrm{DIC}^{\mathrm{cf,equib}}$ can be defined as the DIC concentrations when seawater and air are in equilibrium. $[\mathrm{DIC}]_{\mathrm{deficit}}$ is equal to $\Sigma\mathrm{DIC}^{\mathrm{equib}}$ - $\Sigma\mathrm{DIC}^{\mathrm{cf,equib}}$. This case is first considered for an ocean that is in equilibrium with the atmosphere before being subjected to an OAE intervention and then for an ocean in disequilibrium with the atmosphere before the intervention. This allows one to elucidate what factors affect the timescale for achieving $\mathrm{CDR}^{\mathrm{max}}$ most strongly, and whether this timescale changes for over- or undersaturated cases.

4.1.1. Case 1.1: Starting from an equilibrated surface ocean

In case 1.1, DIC in the surface ocean is in equilibrium with the atmosphere before being perturbed. Then the counterfactual is a time-invariant equilibrium, i.e. equation (3) simplifies to $\partial\mathrm{DIC}^{\mathrm{cf}}(t)/\partial t = 0$ or $\mathrm{DIC}^{\mathrm{cf}} = \mathrm{DIC}^{\mathrm{cf,equib}} = \mathrm{const}$.

In a simulation that is referred to as the Base case, a box thickness of 10 m, typical values for surface ocean temperature, salinity, DIC, and alkalinity (Lauvset et al. 2016), the global average wind speed of Archer & Jacobsen (2005), and an atmospheric $p\mathrm{CO}_2$ of 416 ppm were assumed (Table 1). The CO_2 air-sea flux parameterization of Nightingale et al. (2000) was used and an alkalinity perturbation of 100 μM was applied throughout the volume of the idealized surface ocean. In sensitivity simulations these assumptions were varied systematically.

In the base case, CDR(t) increases steeply for the first 200 days followed by a more gradual increase toward $\mathrm{CDR}^{\mathrm{max}}$ at around 600 days (Figure 1). Timescales toward achieving 50%, 90%, and 99% of $\mathrm{CDR}^{\mathrm{max}}$ are 120, 368, and 703 days, respectively (Table 2). The sensitivity simulations illustrate how these timescales are affected by different parameterizations of the air-sea flux of CO_2, the box thickness, the magnitude of the gas-exchange coefficient k, the wind speed, and the size of the alkalinity perturbation (Table 1).

The volume-normalized CDR(t) and timescales to $\mathrm{CDR}^{\mathrm{max}}$ are almost insensitive to the choice of the gas-exchange parameterization among the 5 tested (Figure 1a, Table 2). At time 0+ (immediately after the alkalinity perturbation), the instantaneous air-sea flux of CO_2 is largest when using the parameterization of McGillis et al. (2004) and smallest when using the parameterization of Wanninkhof et al. (2009), but the differences between parameterizations quickly decrease (Figure 1b) because the magnitude of the flux depends inversely on DIC, which rises slightly faster in the run with the largest flux than in the runs with smaller fluxes. This leads to a convergence of instantaneous fluxes around day 200 followed by a slight temporary divergence where the run with the lowest initial flux experiences a slightly larger flux than the others. In practical terms, the choice of gas exchange parameterization appears comparatively small for the evolution of CDR(t) given the almost negligible differences in this quantity, at least for the average wind speed applied here.

The choice of box thickness, Δz, has a much larger impact on the timescales to $\mathrm{CDR}^{\mathrm{max}}$ and on the magnitude of the flux (Figure 1a,b, Table 2). As should be obvious from the model set-up, $\mathrm{CDR}^{\mathrm{max}}$ (but not the volume-normalized $\mathrm{CDR}^{\mathrm{max}}$) and the timescales change in a linear fashion with changes in box thickness.

The impacts of perturbing the wind speed and the gas-exchange coefficient by +/- 50% are shown on Figure 1c,d. Perturbations of the wind speed have the largest effect. A 50% decrease in wind speed increases the timescales to CDR^{max} by over a factor of 3 and a 50% increase in wind speed cuts the timescales by more than half (Table 2). The impact of changes in the gas-exchange coefficient are smaller. An increase by 50% leads to a decrease in timescales by about 33% while a decrease by 50% leads to an increase in timescales by about 50% (Table 2). These are comparable to the effect due to +/-50% in box thickness. Given that the gas exchange coefficient is probably know to better than +/-50% while the thickness of the surface mixed layer and the wind speed encountered by a parcel of surface water can easily vary by more than +/-50%, the latter two should be considered larger contributors to the uncertainty in flux equilibration timescales.

Lastly, when changing the magnitude of the alkalinity perturbation by +/- 50%, the timescales toward CDR^{max} change by 10%, 7% and 5% for $t_{50\%}$, $t_{90\%}$, and $t_{99\%}$, respectively (Table 2).

4.1.2. Case 1.2: Starting from disequilibrium

In the more general case 1.2, DIC is over- or undersaturated before the alkalinity perturbation (Table 1) allowing an assessment of whether this affects the timescale of CO_2 equilibration. In this case, the counterfactual is non-trivial and must be explicitly calculated as it evolves in time. $[DIC]_{deficit}$ and CDR^{max} are not affected by the initial conditions and equal to the equilibrium base case (Case 1.1) regardless of the degree of over- or undersaturation.

The timescales of air-sea equilibration are different to those in the equilibrium case (Figure 2a, Table 2). In the most oversaturated case (run 17), equilibration occurs the fastest with 50% of maximum efficiency ($t_{50\%}$) reached within 82 days. This is 122 days before the same equilibration benchmark is reached in the most undersaturated case (run 14) where $t_{50\%}$ is 204 days. The differences are asymmetric in that oversaturation by 200 ppm (run 17) shortens $t_{50\%}$ by 38 days while undersaturation by 200 ppm (run 14) prolongs $t_{50\%}$ by 84 days compared to the equilibrium case (run 1). The differences in equilibration timescales arise from differences in the net air-sea flux (Figure 2b). For the first 100 days, the net flux is largest in the most oversaturated case and smallest in the most undersaturated case until, at some point between 100 and 200 days, the flux curves intersect and the initially largest flux becomes the smallest. The shape of the instantaneous air-sea net flux curves is qualitatively different between the over- and undersaturated cases: they are concave everywhere in the oversaturated cases but switch from convex to concave in the undersaturated ones (Figure 2b).

To understand why the net fluxes are different qualitatively and in magnitude, it is helpful to visualize CDR(*t*) as the difference between DIC concentrations in the realistic versus corresponding counterfactual cases (Figure 2c) and the net flux as the difference between the air-sea fluxes in the realistic versus corresponding counterfactual cases (Figure 2d). The area between the realistic and counterfactual DIC curves (Figure 2c), i.e. the volume-normalized CDR(*t*), is obviously growing faster during the first 100 days in the oversaturated case (green) than in the undersaturated case (blue). Due to the non-linearity of the carbonate system, the instantaneous net flux, i.e. the difference between the realistic and counterfactual air-sea fluxes (Figure 2d), is larger in the oversaturated case (green) than in the undersaturated one (blue). The lack of symmetry in net air-sea fluxes between the over- and undersaturated cases may seem surprising because the air-sea flux parameterization itself is symmetric, i.e. $F(\Delta pCO2) = F(-\Delta pCO2)$. However, one has to keep in mind that the net flux is the difference of the air-sea fluxes of the realistic and counterfactual cases which breaks the symmetry.

4.1.3 Case 1 summary

The simplest case of the highly idealized model (case 1.1) yields timescales for the net air-sea flux that are consistent with the estimates of air-sea equilibration from Jones et al. (2014) who reported a global ocean median timescale of 4.4 ± 3.4 months. Uncertainties in wind speed and in the depth of the actively mixed surface layer are the largest sources of error in the timescale toward achieving CDR^{max} followed by uncertainties in the gas-exchange coefficient k. The choice of the air-sea flux parameterization (among the 5 common parameterizations tested here; see Wanninkhof et al. 2009) are small by comparison, at least for the average windspeed used here. For an over- or undersaturated surface ocean (case 1.2) the timescales toward CDR^{max} are strongly affected by the degree of over- or undersaturation. This calls into question the notion that an idealized net uptake curve, i.e. an individual realization of CDR(*t*), can be used as a generalizable curve and linearly combined with others as suggested by Zhou et al. (2025) and Yankovsky et al. (2024).

4.2. Case 2: A spatially resolved surface ocean with horizontal dispersion and vertical exchange

In case 2, a horizontally resolved, inhomogeneous surface ocean with explicit inclusion of horizontal dispersion and vertical mixing is examined. Because horizontal dispersion is assumed to be isotropic, the two horizontal dimensions can be collapsed into one dimension *r* which measures the distance from the injection site, as follows. Without any loss of generality, $\mathrm{DIC}(\mathbf{x},t)$ can be written in polar coordinates as $\mathrm{DIC}(\mathbf{r},t)$ where $\mathbf{r} = (r,\alpha)$. Since for any time *t* and distance from the injection site *r*, $\mathrm{DIC}(r,\alpha,t) = \mathrm{DIC}(r,\beta,t)$ regardless of the values of α and β, the DIC distribution is fully characterized by $\mathrm{DIC}(r,t)$.

One can introduce $\underline{\mathrm{DIC}}(r,t)$ as the integral over all angles, i.e.

$$\underline{\mathrm{DIC}}(r,t) = \int_0^{360} \mathrm{DIC}(r,\alpha,t)\, d\alpha = 2\pi\, \mathrm{DIC}(r,\alpha,t) \qquad (5)$$

and an analogous integral for Alk. Then the spatio-temporal evolutions of DIC and Alk are fully described by

$$\partial \underline{\mathrm{DIC}}(r,t)/\partial t = -\, k_h\, \partial^2\, \underline{\mathrm{DIC}}(r,t)/\partial r^2 - \tau_v\, (\underline{\mathrm{DIC}}(r,t) - \underline{\mathrm{DIC}}^{deep}) + \underline{F}\ , \text{ and} \qquad (6)$$

$$\partial \underline{\mathrm{Alk}}(r,t)/\partial t = -\, k_h\, \partial^2\, \underline{\mathrm{Alk}}(r,t)/\partial r^2 - \tau_v\, (\underline{\mathrm{Alk}}(r,t) - \underline{\mathrm{Alk}}^{deep}), \qquad (7)$$

where τ_v is the vertical mixing timescale, $\underline{\mathrm{DIC}}^{deep}$ and $\underline{\mathrm{Alk}}^{deep}$ are the angular integrals of DIC and alkalinity below the surface layer (defined as in equation 5), and

$$\underline{F} = 2\pi\, F(T,S,\underline{\mathrm{Alk}}(r,t)/2\pi,\underline{\mathrm{DIC}}(r,t)/2\pi,pCO_2^{air}).$$

4.2.1. Case 2.1 Starting from an equilibrated ocean without vertical exchange

In case 2.1, seawater is again assumed to be in equilibrium with the atmosphere before being perturbed, and vertical exchange is neglected. This implies again that the counterfactual is a time-invariant equilibrium. The question to be addressed with this model set up is whether the rate of horizontal dispersion affects the timescales of CDR realization.

In base case 2.1 (run 18), input parameters were chosen to be the same as in base case 1.1 with the addition of a horizontal diffusivity coefficient $K_h = 80\ m^2/s$. Qualitatively, CDR(*t*) evolves similar as in all the previous simulations for case 1 (Figure 3, blue line). The volume-normalized CDR^{max}

is the same for base cases 2.1 and 1.1, but the timescales are shorter in base case 2.1 (Table 2). Some differences in timescales are to be expected, given the distinct model set up. The sensitivities to changes in the thickness of the surface layer, the horizontal diffusivity, and the size of the alkalinity perturbation (Table 1) are examined and reported in Table 2. As one would expect, changing the layer thickness (run 19) has no effect on normalized CDR^{max}, but strongly affects the timescales. As in case 1.1, the timescales are essentially proportional such that halving the layer thickness also cuts the timescales in half (Table 2). Doubling or halving the alkalinity perturbation (runs 22 and 23) does not affect the timescales in this model set-up (Table 2), but may result in differences in air-sea flux if the perturbation were sustained rather than instantaneous.

Not necessarily obvious a priori is the result that doubling or halving the horizontal dispersion coefficient (runs 20 and 21) does not have any effect on the timescales (Table 2). It follows that a faster dispersion of the initial alkalinity perturbation, while leading to smaller differences in surface ocean alkalinity and smaller local air-sea flux differences between the realistic and counterfactual simulations, does not affect the trajectory of CDR(t) or the time scale in this idealized model. In other words, in the absence of vertical exchange processes, smaller local fluxes due to faster dispersion are perfectly balanced by the larger surface area over which these fluxes occur. It is possible that for a sustained perturbation, air-sea flux and equilibration timescales would become sensitive to the magnitude of horizontal dispersion because larger alkalinity and DIC gradients would develop for which the non-linearities of the carbonate system would become meaningful. Overall, the model behavior in case 2.1 is consistent with case 1.1.

4.2.2. Case 2.2: Considering vertical mixing

Case 2.2 is further generalized by considering vertical mixing and imposing a vertical gradient in background DIC (but not in background alkalinity). It follows that surface DIC concentrations in the counterfactual are not time invariant. The surface layer is assumed to be in equilibrium with the atmosphere before the alkalinity addition. This case illustrates how the efficiency is reduced by alkalinity loss from the surface due to vertical mixing while accounting for a possible upward mixing of DIC from below.

As one would expect, consideration of surface alkalinity loss due to vertical mixing (runs 24-26) reduces the efficiency drastically (Figure 3). Increasing the vertical mixing timescale τ_V from 10^{-7} s^{-1} (run 24) to 10^{-5} s^{-1} (run 26) reduces the efficiency from 88% to 7.7% (Table 2). The initial slope of the CDR(t) curve is unaffected by the vertical mixing, but the curve saturates faster at lower values of CDR^{max} (Figure 3). Faster saturation decreases the timescales to maximum efficiency.

Imposing a vertical gradient in the background DIC, where the deep DIC is elevated compared to the surface layer, partly counteracts the effect of alkalinity loss. Upward mixing of DIC in excess of the equilibrium concentration creates a situation akin to the oversaturated case 1 (runs 16-17) which has faster equilibration timescales than the equilibrium and undersaturated cases. The upward mixing decreases the CDR timescales while increasing CDR^{max} and the efficiency compared to the analogous case without a vertical DIC gradient (comparing runs 27-28 to run 25, Table 2, Figure 3). If the surface layer was over- or undersaturated before the alkalinity perturbation the efficiency and timescales would be modified further.

4.2.3 Case 2 summary

Case 2.1 shows that, in the absence of vertical exchange processes, the evolution of CDR(t) is unaffected by the rate of horizontal dispersion. Although faster horizontal dispersion dilutes the added alkalinity, or the $[DIC]_{deficit}$, thus decreasing the resulting net air-sea ΔpCO2 and net air-sea flux, it also increases the area affected by the alkalinity addition, or $[DIC]_{deficit}$, which results in a larger surface area over which air-sea flux occurs.

Inclusion of vertical exchange, as one would expect, has a large effect on the efficiency and CDR^{max}. Given that the magnitude of vertical mixing is poorly constrained and that the difference in efficiency between runs 24 and 26 is large enough to turn open-ocean CDR from a viable (run 24) into a non-viable (run 26) endeavor, this aspect is likely the largest uncertainty and most urgent research need.

5. Concluding thoughts

All mCDR technologies rely on removing CO_2 from the atmosphere by inducing a net flux of CO_2 from the atmosphere into the ocean. Crucial aspects for these technologies to be the economically viable are that this flux must be directly attributable to the mCDR intervention and that it is reliably quantified. Purely observation-based quantification is not feasible for the fundamental reason that the carbon removed due to an mCDR intervention is the difference between a real and a hypothetical (counterfactual) state. The latter cannot, by definition, be observed. Quantification must therefore rely on skillful models, i.e. models that have been rigorously validated against observations. The most important uncertainty in the near-term that emerged from the analysis presented in this review is the magnitude of the vertical transport of water with a DIC deficit induced by the intervention. Vertical transport determines how long water with a DIC deficit stays at the surface ocean in contact with the atmosphere where it can effect a flux of CO_2 from air into the ocean. Another major uncertainty is the long-term rebalancing of carbon among Earth's mobile carbon pools.

Box 1: Definitions

CDR/mCDR: Carbon Dioxide Removal (CDR) is the active removal of CO_2 from the atmosphere followed by its long-term storage in reservoirs other than the atmosphere. When CDR relies on the ocean, either for storing CO_2 or as a conduit for extracting CO_2 from the atmosphere, it is referred to as marine CDR (mCDR).

Biotic mCDR: Biotic mCDR approaches rely on a systematic alteration of biologically mediated fluxes.

Abiotic mCDR: Abiotic mCDR approaches do not rely on the manipulation of biological processes.

MRV/MMRV: The process of measuring (or monitoring), reporting, and verifying CDR, including its additionality and durability, is referred to as MRV or MMRV (Oschlies et al. 2023, Doney et al., 2025).

Durability/permanence: Sometimes used interchangeably, durability refers to the timescale of carbon storage in its intended reservoir implying it is long, while permanence refers to long durability, e.g. over 1,000 years.

Leakage: The amount of CO_2 released to the atmosphere from the reservoir that was intended for its long-term storage, for example due to a redistribution between mobile carbon reservoirs.

Efficiency: The ratio between the theoretically possible net CO_2 uptake from the atmosphere due to a CDR intervention and the accomplished net CO_2 uptake that has occurred within a reasonable timeframe.

Counterfactual: The no-intervention scenario that represents the baseline against which to quantify the impact of a given CDR intervention.

Net-zero CO_2 emissions: CO_2 emissions are at net zero when anthropogenic emissions are balanced by (or equal to) anthropogenic removals (IPCC 2023). It is important to note that this definition does not include natural sources and sinks of atmospheric CO_2. In other words, according to this definition, atmospheric CO_2 may continue to rise or may decline even under net-zero CO_2 emissions because of natural sources or sinks. In contrast, the concept of net-zero greenhouse gas emissions is more complicated because the warming potential differs between different gases and thus has to be considered (see Oschlies et al. 2023 for a definition).

Scaling up: Increasing CDR operations to the point where gigatons of CO_2 are being removed per year.

Gigaton of CO_2: One billion metric tons of CO_2. It is equal to 10^9 t CO_2 or 10^{15} g CO_2. One gigaton of CO_2 is equal to 0.273 gigaton of C.

Sequestration potential: The amount of CO_2 that could be removed by a specific CDR approach if implemented at full scale. Sequestration potential is typically related to the IPCC's stated need to remove 10 Gt CO_2/yr from the atmosphere by the middle of this century and 20 Gt/yr by the end of this century.

Acknowledgements: Constructive comments from Dariia Atamanchuk, Lennart Bach, Scott Doney, Ruth Musgrave, Kai Schulz, Steve Rackley, and one anonymous reviewer are gratefully acknowledged. This work was supported by a grant from the NSERC Alliance program, the Ocean Alk-align grant from Carbon to Sea, and a grant from the ICONIQ Ocean Co-lab.

Literature cited

Anderson LA, Sarmiento JL. 1994. Redfield ratios of remineralization determined by nutrient data analysis. Global Biogeochem. Cycles 8:65–80

Archer CL, Jacobson MZ. 2005. Evaluation of global wind power. J. Geophys. Res. 110:D12110. doi:10.1029/2004JD005462

Bach LT. 2024. The additionality problem of Ocean Alkalinity Enhancement. Biogeosciences 21:261–77. doi:10.5194/bg-21-261-2024

Bach LT, Tamsitt V, Gower J, Hurd CL, Raven, JA, Boyd P. 2021. Testing the climate intervention potential of ocean afforestation using the Great Atlantic Sargassum Belt. Nat. Commun. 12:2556

Bach LT, Ho DT, Boyd PW, Tyka MD. 2023. Toward a consensus framework to evaluate air-sea CO_2 equilibration for marine CO_2 removal. Limnol. Oceanogr. Lett. 8:685–91. doi:10.1002/lol2.10330

Bakker DCE, Watson AJ, Law CS. 2001. Southern Ocean iron enrichment promotes inorganic carbon drawdown. Deep-Sea Res. II Top. Stud. Oceanogr. 48:2483–507. doi:10.1016/S0967-0645(01)00005-4

Blunden J, Boyer T, Eds. 2024. "State of the Climate in 2023". Bull. Amer. Meteor. Soc. 105(8):Si–S484. doi:10.1175/2024BAMSStateoftheClimate.1

Boyd PW, Jickells T, Law CS, Blain S, Boyle EA, et al. 2007. Mesoscale iron enrichment experiments 1993–2005: synthesis and future directions. Science 315:612–17. doi:10.1126/science.1131669

Boyd PW, Bach LT, Hurd CL, Paine E, Raven JA, Tamsitt V. 2022. Potential negative effects of ocean afforestation on offshore ecosystems. Nat. Ecol. Evol. 6:675–83. doi:10.1038/s41559-022-01722-1

Butnar I, Lynch J, Vetter S, Gamaralage D, Tang Y, et al. 2024. A review of life cycle assessment methods to inform the scale-up of carbon dioxide removal interventions. Wiley Interdisciplinary Reviews: Energy and Environment 13:e540. https://doi.org/10.1002/wene.540

Caldeira K, Rau GH. 2000. Accelerating carbonate dissolution to sequester carbon dioxide in the ocean: geochemical implications. Geophys. Res. Lett. 27:225–28. doi:10.1029/1999GL002364

Cooley SR, Klinsky S, Morrow DR, Satterfield T. 2023. Sociotechnical considerations about ocean carbon dioxide removal. Annu. Rev. Mar. Sci. 15:41–66

Doney SC, Wolfe WH, McKee DC, Fuhrman JG. 2025. The Science, Engineering, and Validation of Marine Carbon Dioxide Removal and Storage. Annu. Rev. Mar. Sci. 17:55–81

Doney SC, Mitchell KA, Henson SA, Cavan E, DeVries T, et al. 2024. Observational and Numerical Modeling Constraints on the Global Ocean Biological Carbon Pump. Glob. Biogeochem. Cycles 38:e2024GB008156, doi:10.1029/2024GB008156

Eisaman MD, Geilert S, Renforth P, Bastianini L, Campbell K, et al. 2023. Assessing the technical aspects of ocean-alkalinity-enhancement approaches. In Guide to best practices in ocean alkalinity enhancement research, ed. A Oschlies, A Stevenson, LT Bach, K Fennel, REM Rickaby, et al., 2-oae2023:3. Copernicus Publications, State Planet

Fennel K. 2008. Widespread implementation of controlled upwelling in the North Pacific Subtropical Gyre would counteract diazotrophic N_2 fixation. Mar Ecol Prog Ser 371:301–3

Fennel K, Long MC, Algar C, Carter B, Keller D, et al. 2023. Modelling considerations for research on ocean alkalinity enhancement (OAE). In Guide to Best Practices in Ocean Alkalinity Enhancement Research, ed. A Oschlies, A Stevenson, LT Bach, K Fennel, REM Rickaby, et al., chap. 9. Göttingen, Ger.: Copernicus. doi:10.5194/sp-2-oae2023-9-2023

Fennel K, Mattern JP, Doney SC, Bopp L, Moore AM, et al. 2022. Ocean biogeochemical modelling. Nat. Rev. Methods Primers 2:76. doi:10.1038/s43586-022-00154-2

Fennel K. 2025. Simple models for exploring marine Carbon Dioxide Removal. Github doi: 10.5281/zenodo.xxxxxx

Ferderer A, Schulz KG, Riebesell U, Baker KG, Chase Z, Bach LT. 2024. Investigating the effect of silicate- and calcium-based ocean alkalinity enhancement on diatom silicification. Biogeosciences 21:2777–94. doi:10.5194/bg-21-2777-2024

Foteinis S, Andresen J, Campo F, Caserini S, Renforth P. 2022. Life cycle assessment of ocean liming for carbon dioxide removal from the atmosphere. J. Clean. Prod. 370:133309. doi:10.1016/j.jclepro.2022.133309

Frenger I, Landolfi A, Kvale K, Somes CJ, Oschlies A, et al. 2024. Misconceptions of the marine biological carbon pump in a changing climate: thinking outside the “export” box. Glob. Chang. Biol. 30:e17124. doi:10.1111/gcb.17124

Garai P, Banerjee P, Modal P, Saha NC. 2021. Effect of heavy metals on fishes: toxicity and bioaccumulation. J. Clinical Toxicol. 11:1–10. doi:10.35248/2161-0495.21.s18.001

Gattuso J-P, Magnan AK, Bopp L, Cheung WWL, Duarte CM, et al. 2018. Ocean solutions to address climate change and its effects on marine ecosystems. Front. Mar. Sci. 5:337. doi:10.3389/fmars.2018.00337

Gnanadesikan A, Sarmiento JL, Slater RD. 2003. Effects of patchy ocean iron fertilization on atmospheric carbon dioxide and biological production. Glob. Biogeochem. Cycles 17(2)

Guo JA, Strzepek RF, Swadling KM, Townsend AT, Bach LT. 2024. Influence of ocean alkalinity enhancement with olivine or steel slag on a coastal plankton community in Tasmania. Biogeosciences 21:2335–54. doi:10.5194/bg-21-2335-2024

Halliwell GR, Srinivasan A, Kourafalou V, Yang H, Willey D, et al. 2014. Rigorous evaluation of a fraternal twin ocean OSSE system for the open Gulf of Mexico. J. Atmos. Ocean Tech. 31:105–30. doi:10.1175/JTECH-D-13-00011.1

Halloran PR, Bell TG, Burt WJ, Chu SN, Gill S, Henderson C, Ho DT, Kitidis V, La Plante E, Larrazabal M, Loucaides S, Pearce CR, Redding T, Renforth P, Taylor F, Toome K, Torres R and Watson A. 2025. Seawater carbonate chemistry based carbon dioxide removal: towards commonly agreed principles for carbon monitoring, reporting, and verification. Front. Clim. 7:1487138. doi: 10.3389/fclim.2025.1487138

Hartmann J, Suitner N, Lim C, Schneider J, Marín-Samper L, et al. 2023. Stability of alkalinity in ocean alkalinity enhancement (OAE) approaches – consequences for durability of CO_2 storage. Biogeosciences 20:781–802. doi:10.5194/bg-20-781-2023

Harvey LDD. 2008. Mitigating the atmospheric CO_2 increase and ocean acidification by adding limestone powder to upwelling regions. J. Geophys. Res. 113, C04028. doi:10.1029/2007JC004373

He J, Tyka MD. 2023. Limits and CO_2 equilibration of near-coast alkalinity enhancement. Biogeosciences 20:27–43

Henson SA, Laufkötter C, Leung S, Giering SLC, Palevsky HI, Cavan EL. 2022. Uncertain response of ocean biological carbon export in a changing world. Nat. Geosci. 15:248–54

Ho DT, Law CS, Smith MJ, Schlosser P, Harvey M, Hill P. 2006. Measurements of air-sea gas exchange at high wind speeds in the Southern Ocean: implications for global parameterizations. Geophys. Res. Lett. 33:L16611

Ho DT, Law CS, Smith MJ, Schlosser P, Harvey M, Hill P. 2023. Monitoring, reporting, and verification for ocean alkalinity enhancement. In Guide to Best Practices in Ocean Alkalinity Enhancement Research, ed. A Oschlies, A Stevenson, LT Bach, K Fennel, REM Rickaby, et al., chap. 12. Göttingen, Ger.: Copernicus. doi:10.5194/sp-2-oae2023-12-2023

House KZ, House CH, Schrag DP, Aziz MJ. 2007. Electrochemical acceleration of chemical weathering as an energetically feasible approach to mitigating anthropogenic climate change. Environ. Sci. Technol. 41:8464–70. doi:10.1021/es0701816

Humphreys MP, Daniels CJ, Wolf-Gladrow DA, Tyrell T, Achterberg EP. 2018. On the influence of marine biogeochemical processes over CO_2 exchange between the atmosphere and ocean. Mar. Chem. 199:1–11. doi:10.1016/j.marchem.2017.12.006

IPCC (Intergov. Panel Clim. Change). 2018. Summary for policymakers. In Global Warming of 1.5°C: An IPCC Special Report on the Impacts of Global Warming of 1.5°C Above Pre-Industrial Levels and Related Global Greenhouse Gas Emission Pathways, in the Context of Strengthening the Global Response to the Threat of Climate Change, Sustainable Development, and Efforts to Eradicate Poverty, ed. V Masson-Delmotte, P Zhai, H-O Pörtner, D Roberts, J Skea, et al., 3–24. Cambridge, UK: Cambridge Univ. Press. doi:10.1017/9781009157940.001

IPCC (Intergov. Panel Clim. Change). 2023. Summary for policymakers. In Climate Change 2023: Synthesis Report; Contribution of Working Groups I, II and III to the Sixth Assessment Report of the Intergovernmental Panel on Climate Change, ed. H Lee, J Romero, 1–34. Geneva: IPCC. doi:10.59327/IPCC/AR6-9789291691647.001

Jeltsch-Thömmes A, Tran G, Lienert S, Keller D, Oschlies A, Joos F. 2024. Earth system responses to carbon dioxide removal as exemplified by ocean alkalinity enhancement: tradeoffs and lags. Environ. Res. Lett. doi:10.1088/1748-9326/ad4401

Jiao N, Robinson C, Azam F, Thomas H, Baltar F, et al. 2014. Mechanisms of microbial carbon sequestration in the ocean – future research directions. Biogeosciences 11:5285–5306. doi:10.5194/bg-11-5285-2014

Jin X, Gruber N, Frenzel H, Doney SC, McWilliams JC. 2008. The impact on atmospheric CO_2 of iron fertilization induced changes in the ocean's biological pump, Biogeosciences, 5, 385-406

Jones DC, Ito T, Takano Y, Hsu W-C. 2014. Spatial and seasonal variability of the air-sea equilibration timescale of carbon dioxide. Glob. Biogeochem. Cy. 28:1163–78. doi:10.1002/2014GB004813

Jürchott M, Oschlies A, Koeve W. 2023. Artificial upwelling—a refined narrative. Geophys. Res. Lett. 50:e2022GL101870. doi:10.1029/2022GL101870

Karl DM, Letelier RM. 2008. Nitrogen fixation-enhanced carbon sequestration in low nitrate, low chlorophyll seascapes. Mar Ecol Prog Ser 364:257–68

Keller DP, Feng EY, Oschlies A. 2014. Potential climate engineering effectiveness and side effects during a high carbon dioxide-emission scenario. Nat. Commun. 5:3304. doi:10.1038/ncomms4304

Keller, D. P., Lenton, A., Scott, V., Vaughan, N. E., Bauer, N., et al. 2018. The Carbon Dioxide Removal Model Intercomparison Project (CDRMIP): rationale and experimental protocol for CMIP6, Geosci. Model Dev. 11:1133–1160

Kheshgi HS. 1995. Sequestering atmospheric carbon dioxide by increasing ocean alkalinity. Energy 20:915–22. doi:10.1016/0360-5442(95)00035-F

Koweek DA. 2022. Expected limits on the potential for carbon dioxide removal from artificial upwelling. Front. Mar. Sci. 9:841894. doi:10.3389/fmars.2022.841894

Laurent A, Fennel K, Kuhn A. 2021. An observation-based evaluation and ranking of historical Earth system model simulations in the northwest North Atlantic Ocean. Biogeosciences 18:1803–22. doi:10.5194/bg-18-1803-2021

Lauvset SK, Key RM, Olsen A, van Heuven S, Velo A, et al. 2016. A new global interior ocean mapped climatology: the 1° × 1° GLODAP version 2. Earth Syst. Sci. Data 8:325–40. doi:10.5194/essd-8-325-2016

Macreadie PI, Costa MDP, Atwood TB, Friess DA, Kelleway JJ, et al. 2021. Blue carbon as a natural climate solution. Nat. Rev. Earth Environ. 2:826–39. doi:10.1038/s43017-021-00224-1

Mahadevan A. 2016. The impact of submesoscale physics on primary productivity of plankton. Annu. Rev. Mar. Sci. 8:161–84. doi:10.1146/annurev-marine-010814-015912

Martin JH. 1990. Glacial-interglacial CO2 change: the iron hypothesis. Paleoceanography 5:1–13. doi:10.1029/PA005i001p00001

McGillis WR, Edson JB, Hare JE, Fairall CW. 2001. Direct covariance of air-sea CO_2 fluxes. J. Geophys. Res. 106:16729–45

McGillis WR, Edson JB, Zappa CJ, Ware JD, McKenna SP, et al. 2004. Air-sea CO_2 exchange in the equatorial Pacific. J. Geophys. Res. 109:C08S02

McWilliams JC. 2016. Submesoscale currents in the ocean. Proc. R. Soc. A 472:20160117. doi:10.1098/rspa.2016.0117

Montserrat F, Renforth P, Hartmann J, Leermakers M, Knops P, Meysman FJR. 2017. Olivine dissolution in seawater: implications for CO_2 sequestration through enhanced weathering in coastal environments. Environ. Sci. Technol. 51:3960–72. doi:10.1021/acs.est.6b05942

Moras CA, Bach LT, Cyronak T, Joannes-Boyau R, Schulz KG. 2022. Ocean alkalinity enhancement – avoiding runaway $CaCO_3$ precipitation during quick and hydrated lime dissolution. Biogeosciences 19:3537–57. doi:10.5194/bg-19-3537-2022

Mouw CB, Barnett A, McKinley GA, Gloege L, Pilcher D. 2016. Global ocean particulate organic carbon flux merged with satellite parameters. Earth Syst. Sci. Data 8:531–41. doi:10.5194/essd-8-531-2016

NASEM (Natl. Acad. Sci. Eng. Med.). 2022. A research strategy for ocean-based carbon dioxide removal and sequestration. Rep., NASEM, Washington, DC. doi:10.17226/26278

Nightingale PD, Malin G, Law CS, Watson AJ, Liss PS, et al. 2000. In situ evaluation of air-sea gas exchange parameterizations using novel conservative and volatile tracers. Glob. Biogeochem. Cycles 14:373–87

Noh K-M, Liu X, Stock CAA, Dunner, JPP. 2024. Assessing the Effectiveness of Ocean Iron Fertilization for the Carbon-Uptake Efficacy. ESS Open Archive. doi:10.22541/essoar.173557508.81096097/v1

Oschlies A. 2009. Impact of atmospheric and terrestrial CO_2 feedbacks on fertilization-induced marine carbon uptake. Biogeosciences 6:1603–13. doi:10.5194/bg-6-1603-2009

Oschlies A, Pahlow M, Yool A, Matear RJ. 2010. Climate engineering by artificial ocean upwelling—channelling the sorcerer's apprentice. Geophys. Res. Lett. 37:L04701

Oschlies A, Stevenson A, Bach LT, Fennel K, Rickaby REM, et al. 2023. Guide to Best Practices in Ocean Alkalinity Enhancement Research (OAE Guide 23). State Planet: SP, 2-oae202. 1–242. doi:10.5194/sp-2-oae2023

Oschlies A, Bach LT, Fennel K, Gattuso J-P, Mengis N. 2025. Perspectives and challenges of marine carbon dioxide removal. Front. Clim. 6:1506181. doi:10.3389/fclim.2024.1506181

Palter JB, Cross J, Long MC, Rafter PA, Reimers CE. 2023. The science we need to assess marine carbon dioxide removal. Eos 104. doi:10.1029/2023EO230214

Rau GH. 2008. Electrochemical splitting of calcium carbonate to increase solution alkalinity: implications for mitigation of carbon dioxide and ocean acidity. Environ. Sci. Technol. 42:8935–40. doi:10.1021/es800366q

Rau GH, Caldeira K. 1999. Enhanced carbonate dissolution: a means of sequestering waste CO_2 as ocean bicarbonate. Energy Convers. Manag. 40:1803–13. doi:10.1016/S0196-8904(99)00071-0

Rau GH, Carroll SA, Bourcier WL, Singleton MJ, Smith MM, Aines RD. 2013. Direct electrolytic dissolution of silicate minerals for air CO2 mitigation and carbon-negative H_2 production. Proc. Natl. Acad. Sci. USA 110:10095–10100. doi:10.1073/pnas.1222358110

Redfield AC, Ketchum BH, Richards FA. 1963. The influence of organisms on the composition of sea-water. In The Sea, ed. MN Hill, 2:26–77. Interscience, New York

Renforth P. 2019. The negative emission potential of alkaline materials. Nat. Comms. 10:1401. doi:10.1038/s41467-019-09475-5

Renforth P, Baltruschat S, Peterson K, Mihailova B, Hartmann J. 2022. Using ikaite and other hydrated carbonate minerals to increase ocean alkalinity for carbon dioxide removal and environmental remediation. Joule 6:2674–79. doi:10.1016/j.joule.2022.11.001

Renforth P, Henderson G. 2017. Assessing Ocean alkalinity for carbon sequestration. Rev. Geophys. 55:636–74. doi:10.1002/2016RG000533

Ricour F, Guidi L, Gehlen M, DeVries T, Legendre L. 2023. Century-scale carbon sequestration flux throughout the ocean by the biological pump. Nat. Geosci. 16:1105–13

Roberts KE, Harrison CS, Rohr TW, Raven M, Diamond MA, et al. 2024. Potential impacts of climate interventions on marine ecosystems. ESS Open Archive. doi: 10.22541/essoar.173482381.11257447/v1

Saha P, Meeder J, Singh S, Ramesh S, Nippe M, Kwabi DG. 2024. Enabling light-driven CO_2 removal from seawater using metastable photoacids. J. Phys. Chem. C 128:4914–23. doi:10.1021/acs.jpcc.3c08306

Sarmiento JL, Gruber N, Brzezinski MA, Dunne JP. 2004. High-latitude controls of thermocline nutrients and low latitude biological productivity. Nature 427:56–60

Schulz KG, Bach LT, Dickson AG. 2023. Seawater carbonate chemistry considerations for ocean alkalinity enhancement research: theory, measurements, and calculations. In Guide to Best Practices in Ocean Alkalinity Enhancement Research, ed. A Oschlies, A Stevenson, LT Bach, K Fennel, REM Rickaby, et al., 2-oae2023:2. Copernicus Publications, State Planet. doi:10.5194/sp-2-oae2023-2-2023

Schwinger J, Bourgeois T, Rickels W. 2024. On the emission-path dependency of the efficiency of ocean alkalinity enhancement. Environ. Res. Lett. 19:074067. doi:10.1088/1748-9326/ad5a27

Seo H, Schretter J, Massen-Hane M, Hatton TA. 2024. Visible Light-Driven CO2 Capture and Release Using Photoactive Pyranine in Water in Continuous Flow. J. Am. Chem. Soc. 146(39):26777–85. doi:10.1021/jacs.4c07278

Sheppard EJ, Hurd CL, Britton DD, Reed DC, Bach LT. 2023. Seaweed biogeochemistry: global assessment of C:N and C:P ratios and implications for ocean afforestation. J. Phycol. 59:879–92. doi:10.1111/jpy.13381

Siegel DA, DeVries T, Doney SC, Bell T. 2021. Assessing the sequestration time scales of some ocean-based carbon dioxide reduction strategies. Environ. Res. Lett. 16:104003. doi:10.1088/1748-9326/ac0be0

Strong AL, Cullen JJ, Chisholm SW. 2009. Ocean fertilization: science, policy, and commerce. Oceanography 22(3):236–61. doi:10.5670/oceanog.2009.83

Sunda WG. 1997. Control of dissolved iron concentrations in the world ocean: a comment. Mar. Chem. 57:169–72

Sunda WG, Huntsman SA. 1995. Iron uptake and growth limitation in oceanic and coastal phytoplankton. Mar. Chem. 50:189–206

Tyka MD. 2025. Efficiency metrics for ocean alkalinity enhancement under responsive and prescribed atmospheric pCO_2 conditions. Biogeosciences 22: 341–353. https://doi.org/10.5194/bg-22-341-2025

Wang, H., Pilcher, D. J., Kearney, K. A., Cross, J. N., Shugart, et al. 2023. Simulated impact of ocean alkalinity enhancement on atmospheric CO2 removal in the Bering Sea, Earth's Future, 11, e2022EF002816

Wang B, Fennel K. 2024. Distinct sources of uncertainty in simulations of the ocean biological carbon pump at different depths. Commun Earth Environ 5:395. doi:10.1038/s43247-024-01561-x

Wang B, Laurent A, Pei Q, Sheng J, Atamanchuk A, Fennel, K. 2025. Maximizing the detectability of Ocean Alkalinity Enhancement (OAE) while minimizing its exposure risks: Insights from a numerical study. Earth's Future, 13, e2024EF005463

Wanninkhof R, Asher WE, Ho DT, Sweeney C, McGillis WR. 2009. Advances in quantifying air-sea gas exchange and environmental forcing. Annu. Rev. Mar. Sci. 1:213–244

Watson AJ, Boyd PW, Turner SM, Jickells TD, Liss PS. 2008. Designing the next generation of ocean iron fertilization experiments. Mar. Ecol. Prog. Ser. 364:303–9. doi:10.3354/meps07552

Williamson P, Gattuso J-P. 2022. Carbon removal using coastal blue carbon ecosystems is uncertain and unreliable, with questionable climatic cost-effectiveness. Front. Clim. 4:853666. doi:10.3389/fclim.2022.853666

Yamamoto K, DeVries T, Siegel DA. 2024. Metrics for quantifying the efficiency of atmospheric CO2 reduction by marine carbon dioxide removal (mCDR). Environ. Res. Lett. 19:104052. doi:10.1088/1748-9326/ad7477

Yang AJK, Timmermans M-L. 2024. Assessing the effective settling of mineral particles in the ocean with application to ocean-based carbon-dioxide removal. Environ. Res. Lett. 19:024035. doi:10.1088/1748-9326/ad2236

Yankovsky E, Zhou M, Tyka M, Bachmann S, Ho DT et al. 2024. Impulse response functions as a framework for quantifying ocean-based carbon dioxide removal. EGUsphere [preprint]. doi:10.5194/egusphere-2024-2697

Yool A, Shepherd JG, Bryden HL, Oschlies A. 2009. Low efficiency of nutrient translocation for enhancing oceanic uptake of carbon dioxide. J. Geophys. Res. 114(C8):C08009. doi:10.1029/2008JC004792

Yoon J-E, Yoo K-C, Macdonald AM, Yoon H-I, Park K-T, et al. 2018. Reviews and syntheses: ocean iron fertilization experiments – past, present, and future looking to a future Korean Iron fertilization experiment in the Southern Ocean (KIFES) project. Biogeosciences 15:5847–89. doi:10.5194/bg-15-5847-2018

Yu L, Fennel K, Wang B, Laurent A, Thompson KR, Shay LK. 2019. Evaluation of nonidentical versus identical twin approaches for observation impact assessments: an ensemble-Kalman-filter-based ocean assimilation application for the Gulf of Mexico. Ocean Sci. 15:1801–14. doi:10.5194/os-15-1801-2019

Zeebe RE, Wolf-Gladrow DA. 2001. CO2 in seawater: equilibrium, kinetics, isotopes. Elsevier Oceanographic Series, Vol. 65. 346 pp.

Zhou M, Tyka MD, Ho DT, Yankovsky E, Bachmann S, et al. 2025. Mapping the global variation in the efficiency of ocean alkalinity enhancement for carbon dioxide removal. Nat. Clim. Chang. 15:59–65. doi:10.1038/s41558-024-02179-9

Tables

Table 1

Run #	Short description	Δz (m)	T (°C)	S	U10 (m/s)	DIC^{cf} (uM)	Alk^{cf} (uM)	pCO_2^{air} (ppm)	$pCO_2(0+)$ (ppm)	ΔAlk (uM)	Gas exchange parametrization
Case 1.1, Assumptions: homogenous volume (no dispersion); no spatial dimension, just time; infinite atmosphere; ocean and atmosphere are in equilibrium before intervention, thus counterfactual is time-invariant equilibrium											
1	Base case	10	20	35	6.64	2050	2300	416	281	100	Nightingale et al. (2000)
2-5	Gas exchange parametrization	Same as Base case except for gas exchange parametrizations; run 2: McGillis et al. (2001), run 3: McGillis et al. (2004), run 4: Ho et al. (2006), run 5: Wannikhof et al. (2009)									
6-7	Box thickness	Same as Base case 1.1 except for Δz; run 6: $\Delta z = 5$ m, run 7: $\Delta z = 15$ m									
8-9	Gas exchange coefficient k	Same as Base case 1.1 except for gas exchange coefficient; run 8: k is smaller by 50%, run 9: k is larger by 50%									
10-11	Wind speed	Same as Base case 1.1 except for wind speed; run 10: U10 is smaller by 50%, run 11: U10 is larger by 50%									
12-13	Alkalinity perturbation	Same as Base case 1.1 except for ΔAlk: run 12: ΔAlk is smaller by 50%, run 13: ΔAlk is larger by 50%									
Case 1.2, Assumptions: same as case 1.1 except that ocean and atmosphere do not start from equilibrium; counterfactual is non-trivial and evolves in time											
14-17	Starting from air-sea disequilibrium	Same as base 1.1 case except for initial DIC; initial $\Delta pCO2$ between ocean and atmosphere is -200 ppm (run 14, $DIC^{cf} = 1910$), -100 ppm (run 15, $DIC^{cf} = 1990$), 100 ppm (run 16, $DIC^{cf} = 2090$), and 200 ppm (run 17, $DIC^{cf} = 2120$)									
Case 2.1, Assumptions: surface ocean with horizontal space and time dimensions; since dispersion is assumed to be isotropic, spatial distribution patterns can be described mathematically with just one spatial dimension; counterfactual is time-invariant equilibrium											
18	Base case	Same parameters as Base case 1.1 with addition of a horizontal diffusivity parameter $K_h = 80$ m^2/s									
19	Box thickness	Same as Base case 2.1 except for $\Delta z = 5$ m									
20-21	Horizontal diffusivity K_h	Same as Base case 2.1 except for horizontal diffusivity; run 20: $K_h = 40$ m^2/s, run 21: $K_h = 160$ m^2/s									
22-23	Alkalinity perturbation	Same as Base case 2.1 except for ΔAlk: run 22: $\Delta Alk = 50$ uM, run 23: $\Delta Alk = 200$ uM									
Case 2.2, Assumptions: 2-layer ocean with horizontal, vertical, and time dimensions; vertical gradient in DIC is imposed; vertical mixing is parameterized; horizontal dispersion is isotropic; counterfactual is not a time-invariant equilibrium anymore and needs to be solved											
24-26	Vertical mixing τ_v	Same as Base case 2.1 except for vertical mixing timescale; run 24: $\tau_v = 10^{-7}$ s^{-1}, run 25: $\tau_v = 10^{-6}$ s^{-1}, run 26: $\tau_v = 10^{-5}$ s^{-1} (no vertical DIC gradient)									
27-28	Vertical DIC gradient	Same as run 25 with a vertical DIC gradient imposed; run 27: $DIC^{deep} = 2150$ uM, run 28: $DIC^{deep} = 2250$ uM									

Table 2

Case #	Run #	CDR^{max} (uM)	$\varepsilon_{99\%}$ (%)	$t_{50\%}$ (d)	$t_{90\%}$ (d)	$t_{99\%}$ (d)		Case #	Run #	CDR^{max} (uM)	$\varepsilon_{99\%}$ (%)	$t_{50\%}$ (d)	$t_{90\%}$ (d)	$t_{99\%}$ (d)
1.1	1	83.7	99	120	368	703		1.2	15	83.7	99	152	420	764
1.1	2	83.7	99	132	404	773		1.2	16	83.7	99	98.1	328	655
1.1	3	83.7	99	117	359	686		1.2	17	83.7	99	82.5	296	614
1.1	4	83.7	99	123	376	720		2.1	18	83.3	98.5	95.1	316	631
1.1	5	83.7	99	136	417	798		2.1	19	83.3	98.7	47.5	158	315
1.1	6	83.7	99	60	184	352		2.1	20	83.3	98.5	95.1	316	631
1.1	7	83.7	99	180	552	1060		2.1	21	83.2	98.5	95.1	316	629
1.1	8	83.7	99	240	736	1410		2.1	22	83.2	98.4	95.1	316	631
1.1	9	83.7	99	80	245	469		2.1	23	83.5	98.7	95.1	316	631
1.1	10	83.7	99	405	1240	2380		2.2	24	74.4	88.1	85.0	282	561
1.1	11	83.7	99	56.8	174	333		2.2	25	38.1	45.1	43.5	145	289
1.1	12	83.7	99	108	342	668		2.2	26	6.48	7.67	7.41	24.5	49.1
1.1	13	83.7	99	132	393	738		2.2	27	42.8	50.6	44.8	136	259
1.2	14	83.7	99	204	495	846		2.2	28	47.2	55.9	44.9	124	226

Table 2: Values of CDR^{max}, the timescales for CDR to reach 50%, 90%, and 99% of CDR^{max}, $t_{50\%}$, $t_{90\%}$, and $t_{99\%}$, and the efficiency at $t_{99\%}$, $\varepsilon_{99\%}$. CDR^{max} is normalized by the volume to which the alkalinity perturbation was applied and the alkalinity perturbation.

Figures

Figure 1

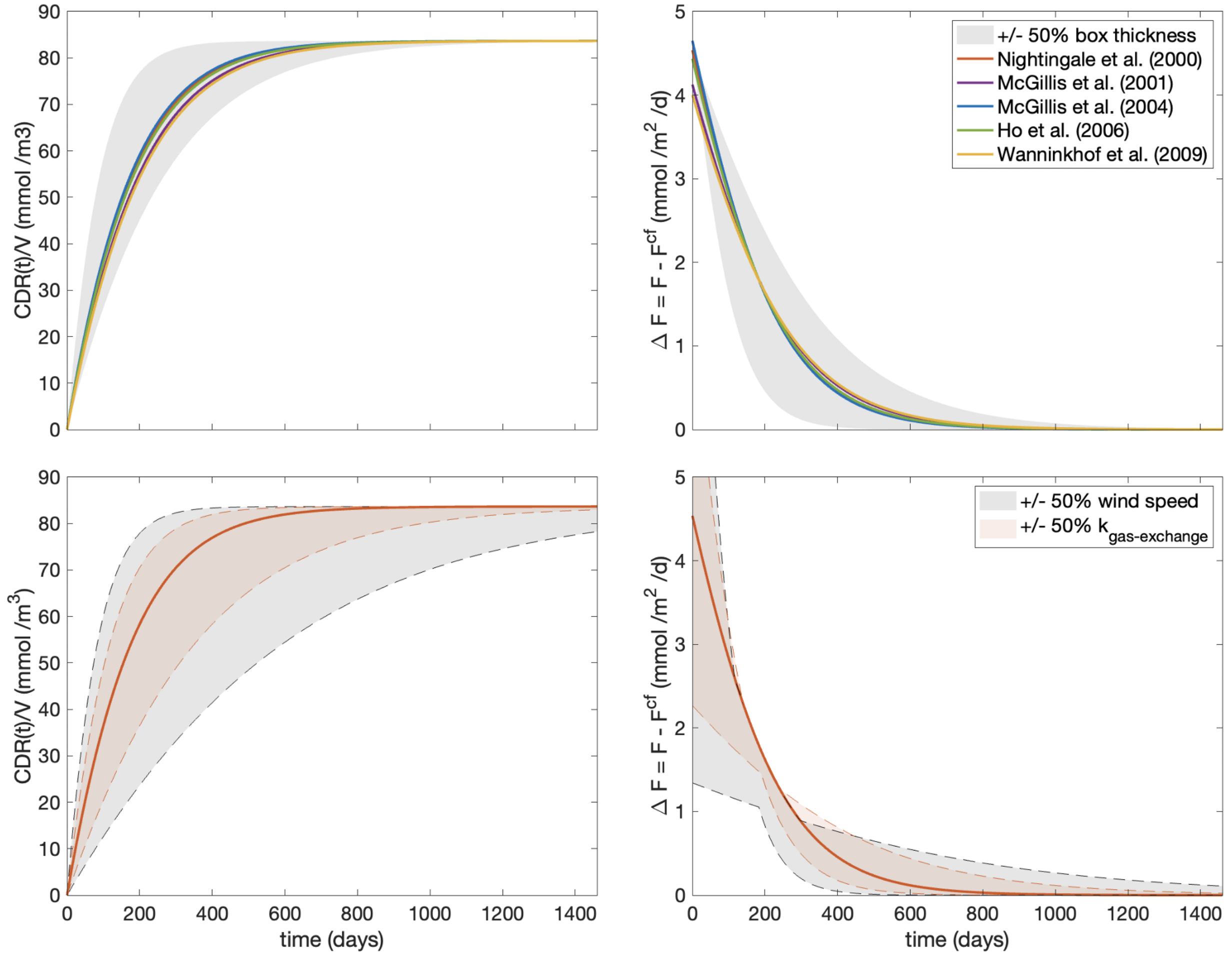

Figure 1: a) Volume-normalized CDR(*t*) for case 1.1, runs 1-11 (see Table 1) plotted over the first 4 years from the alkalinity perturbation at t = 0. Range of values for +/- 50% of box thickness is shown by the gray area. b) Same as a) but for the instantaneous net air-sea flux of CO_2. c) Volume-normalized CDR(*t*) for the base case with shaded areas showing the range of values for +/- 50% of the wind speed (gray) and gas exchange coefficient (red). d) Same as c) but for the instantaneous net air-sea flux of CO_2. Positive air-sea flux signifies a flux into the ocean (from air to sea).

Figure 2

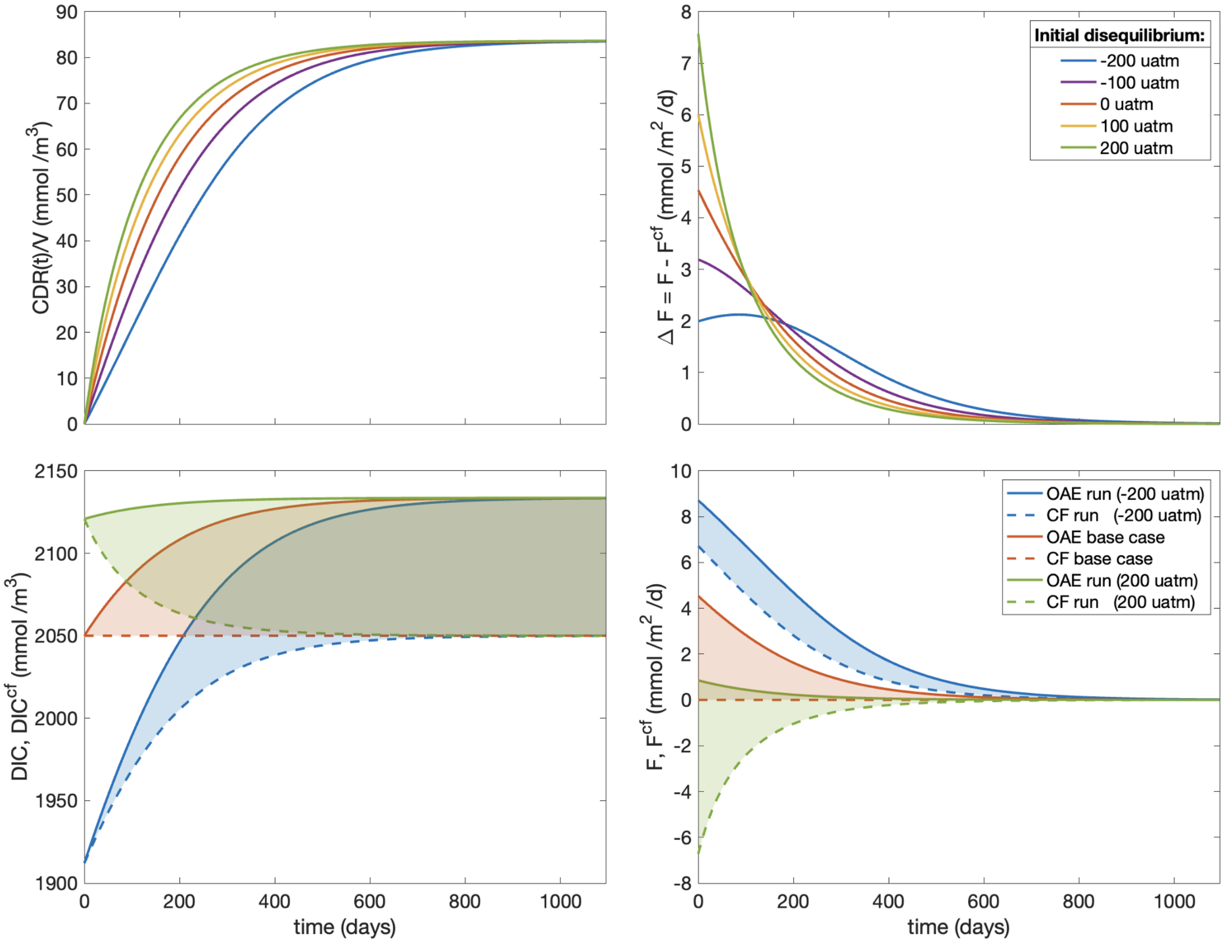

Figure 2: a) Volume-normalized CDR(*t*) for case 1.2, runs 14-17 and the Base case 1.1, run 1 (see Table 1) plotted over the first 3 years from alkalinity perturbation at *t* = 0. b) Same as in a) but for the instantaneous net air-sea flux of CO_2. c) DIC concentrations for OAE runs (solid lines) and corresponding counterfactuals (dashed lines) with shaded area representing CDR(*t*)/V for run 14 (blue), run 1 (red), and run 17 (green). Positive air-sea flux signifies a flux into the ocean (from air to sea).

Figure 3

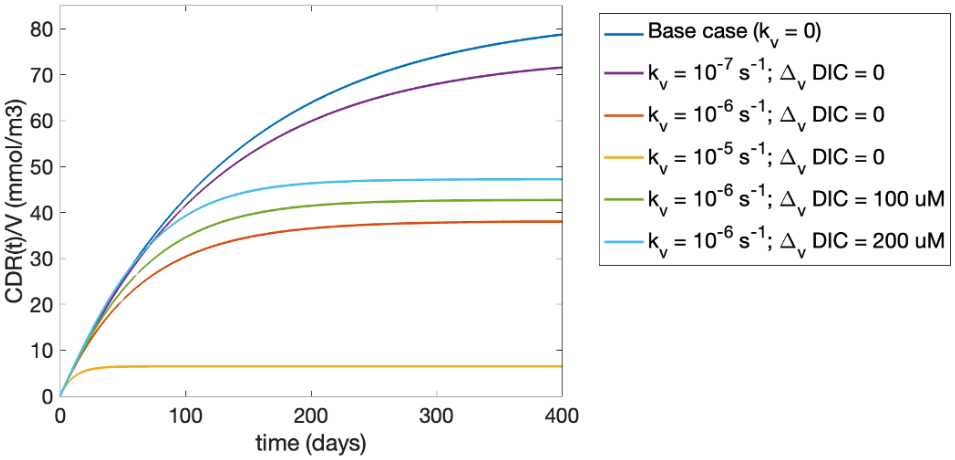

Figure 3: Volume-normalized CDR(*t*) for case 2.1 (base case, run 18) and case 2.2 (runs 24-28).